PROCEEDINGS A

royalsocietypublishing.org/journal/rspa

Research

Cite this article: Jones IS, Movchan NV, Movchan AB. 2023 Gravity-induced dispersion in a chiral waveguide: transient regimes and imperfect temporal interfaces. *Proc. R. Soc. A* **479**: 20230338.
https://doi.org/10.1098/rspa.2023.0338

Received: 14 May 2023
Accepted: 9 August 2023

Subject Areas:
applied mathematics, mathematical modelling, wave motion

Keywords:
gravity-induced dispersion, chiral waveguide, temporal interfaces, transient regimes

Author for correspondence:
N. V. Movchan
e-mail: nvm@liverpool.ac.uk

One contribution to a special feature 'Mathematical theory and applications of multiple wave scattering' organised by guest editors Luke G. Bennetts, Michael H. Meylan, Malte A. Peter, Valerie J. Pinfield and Olga Umnova.

THE ROYAL SOCIETY PUBLISHING

Gravity-induced dispersion in a chiral waveguide: transient regimes and imperfect temporal interfaces

I. S. Jones, N. V. Movchan and A. B. Movchan

Department of Mathematical Sciences, University of Liverpool, Liverpool L69 7ZL, UK

NVM, 0000-0001-9166-1952; ABM, 0000-0001-8902-9923

The paper includes analysis of an elastic chiral waveguide, subjected to gravity, where a coupling between different displacement components is assumed owing to gyroscopic action. The importance of gravity and chirality on the dispersion of waves is demonstrated and behaviour in all regimes, including asymptotic ones, is addressed and linked to the value of the chirality parameter. In the transient regimes, we analyse chiral imperfect temporal interfaces in the waveguide subjected to gravity.

1. Introduction

The emphasis of this paper is on the analysis of gravity-induced waves in a chiral elastic waveguide. For a discrete system, chirality is introduced through a gyroscopic force, exerted by gyroscopic spinners embedded in an elastic structure. Examples of such structures are studied in [1–3]. The formal connection was noted in [4] for models of mechanical gyroscopic systems and models of electromagnetic systems, in the context of the classical work of Lorentz [5] (also, see [6]).

Homogenization leads to a continuum formulation, where gyroscopic forces are represented by the '90-degree rotation' coupling terms. The effect of gravity appears to be important in the context of wave dispersion and wave localization.

Discrete models of vibrations in chiral elastic lattice systems, without the effects of gravity, were discussed in [7], with the focus on wave dispersion. Reference [7] also included ideas of homogenization of chiral elastic media, which were successfully used in [8] to generate one-way elastic edge waves.

Experimental observations and discussion of mechanical chiral systems in the context of Topological Mechanics, are presented in [9].

Detailed analysis of elastic waves in a chiral elastic chain, containing gyroscopic spinners, which includes construction of dynamic Green's matrices and study of localized defect modes, is reported in [10]. In a recent reference [11], the effect of gravity has been analysed for dispersion and localization of waves in discrete chiral elastic waveguides.

Elastic multi-structures, which incorporate elastic beams connected to gyroscopic spinners, were analysed in [12–14] in the framework of linearized models, which capture the gyroscopic coupling, but do not take into account the effect of gravity. These papers include the study of the dynamic response of such systems and the dispersion properties of chiral flexural waveguides. In particular, the paper [12] makes a formal link between waves in the structure, incorporating flexural beams constrained by a periodic system of gyroscopic hinges, and wave dispersion in elastic gyrobeams.

The book [15] presents the mathematical theory of dynamic materials, where the coefficients in the governing equations may change in time. The analysis of wave patterns in structures, which possess spatial and temporal interfaces, is analysed in [16–18]. Causality always holds for physical processes, but interesting wave phenomena are observed when a wave is split at a temporal interface. The energy balance relations for waves in a spatio-temporal material composite is addressed in [19]. The modelling of frontal waves, incorporating the analysis of the transient wave phenomena in structures that have stratification in the temporal dimension, is discussed in [20]. The study of temporal modulation of frontal waves is emphasized, with special regimes being identified where the solution shows growth in time. Imperfect interfaces, across which the displacements are discontinuous, are also considered in [20] for the vector case of chiral elastic systems.

In the present paper, we focus on the effect of gravity on transient regimes in elastic chiral waveguides and analysis of temporal boundary layers. The structure of the paper is as follows. The formulation of the problem and the normalization, which reduces the equations to a non-dimensional form, are discussed in §2. In addition to fully transient modelling, this section also includes the case of time-harmonic vibrations where an analysis of the effects of variation of the main parameters is carried out. Discussion of the case where the gyricty is high is presented in §3, where an additional normalization, related to rapid oscillations, and 'fast time', is introduced. Furthermore, the stationary wave solution is analysed where the spatial evolution of the wave is negligibly small compared to the oscillations in time. Additionally in §4, the boundary layer in the transition regimes is discussed, together with imperfect temporal interfaces, when gyroscopic gyricity is large and gravity is present.

2. The governing equations: transient solutions and normalized representations

Here, the model of elastic waves in a continuum elastic waveguide is considered. The waveguide is characterized by the gyroscopic coupling and subjected to gravity. The questions of normalization of the governing equations appear to be important, especially for the cases when the gyricity, associated with the coupling terms, increases. Waves in a chiral 'meta-waveguide', have been analysed in [1] in the absence of gravity. If the gravity term is introduced in the governing equations, the solution shows significant changes, especially in the transition regimes for small values of time. The periodic discrete system of pendulums, connected by springs, has been analysed in [11] and here we consider the continuum analogue with a focus on transient regimes.

royalsocietypublishing.org/journal/rspa Proc. R. Soc. A 479: 20230338

(a) The continuum equations of the chiral elastic waveguide subjected to gravity

Consider the continuum analogue of the discrete chiral elastic chain positioned along the x-axis. Let $u(x,t)$ and $v(x,t)$ be the longitudinal and transverse displacements, respectively. Consider further, an analogue of the discrete gyroscopic spinner-spring chain, subjected to gravity, with lattice spacing d, similar to the one analysed in [1,11]:

$$m\ddot{\boldsymbol{\mathcal{U}}}_n(t) - d^{-2}\mathrm{diag}(\lambda_1 d^2, \lambda_2 d^2)(\boldsymbol{\mathcal{U}}_{n+1}(t) + \boldsymbol{\mathcal{U}}_{n-1}(t) - 2\boldsymbol{\mathcal{U}}_n(t)) - m\alpha\mathbf{R}\dot{\boldsymbol{\mathcal{U}}}_n(t) + mG\boldsymbol{\mathcal{U}}_n(t) = \mathbf{0}. \tag{2.1}$$

Here, m is the common value of the masses in the chain, $\boldsymbol{\mathcal{U}}_n(t)$ is the displacement of the nodal point n in the horizontal plane, λ_1 is the spring stiffness and λ_2 an induced stiffness perpendicular to the chain [1], d is the inter-mass equilibrium distance, α is the gyricity parameter, and $\mathbf{R}$ is the 90^o clockwise rotation matrix

$$\mathbf{R} = \begin{pmatrix} 0 & 1 \\ -1 & 0 \end{pmatrix}. \tag{2.2}$$

The normalized gravity parameter G is the same as in [11], $G = g/l$, where g is the gravity acceleration and l is the length of the arm of the pendulum in the elementary cell of the waveguide. The term, including the velocity $\dot{\boldsymbol{\mathcal{U}}}_n(t)$ represents the gyroscopic force, which is orthogonal to the velocity vector. The linearized differential equations, describing the motion of a single gyropendulum for small values of the nutation angle, are classical (e.g. [4]). The gyricity parameter α depends on the rate of spin and the moments of inertia, and its evaluation for particular cases, including physical examples, is discussed in detail in [1].

The continuum limit is found by letting $d \to 0$, $m \to 0$ and $\lambda_1 \to \infty$ such that the chiral line density, m/d, and tension, $\lambda_1 d$, are finite. Bulk continuum properties are defined as: the chiral density $\rho = m/d^3$ and Young's modulus $E_1 = \lambda_1/d$. We also use the notation $E_2 = \lambda_2/d$. In the continuum limit

$$\left.\begin{aligned} &\frac{\partial^2 u}{\partial t^2} - \frac{E_1}{\rho}\frac{\partial^2 u}{\partial x^2} - \alpha\frac{\partial v}{\partial t} + Gu = 0 \\ \text{and}\quad &\frac{\partial^2 v}{\partial t^2} - \frac{E_2}{\rho}\frac{\partial^2 v}{\partial x^2} + \alpha\frac{\partial u}{\partial t} + Gv = 0. \end{aligned}\right\} \tag{2.3}$$

When gyroscopic action and gravity are absent (i.e. $\alpha = 0$ and $G = 0$), equation (2.3) is reduced to a system of uncoupled wave equations. When $|\alpha| > 0$, the coupling between $u(x,t)$ and $v(x,t)$ becomes apparent, and the waves along the chiral rod governed by equation (2.3) become dispersive.

(b) Normalization of the governing equations

A canonical system is considered whereby the parameter α is used as a measure of the degree of chirality in the system, while the force owing to gravity is considered to be a constant quantity. Thus equation (2.3) will be solved subject to the initial conditions

$$\left.\begin{aligned} &u(x,0) = Lf_1\left(\frac{x}{L}\right), \quad v(x,0) = Lf_2\left(\frac{x}{L}\right), \\ &\frac{\partial u}{\partial t}(x,0) = c_1 g_1\left(\frac{x}{L}\right) \quad \text{and} \quad \frac{\partial v}{\partial t}(x,0) = c_1 g_2\left(\frac{x}{L}\right). \end{aligned}\right\} \tag{2.4}$$

Here L is defined as a characteristic length introduced in the initial conditions and $c_1 = \sqrt{E_1/\rho}$. The functions f_i and g_i are dimensionless.

Introduce the dimensionless variables:

$$\tilde{x} = \frac{x}{L}, \quad \tilde{t} = \frac{c_1 t}{L}, \quad \tilde{u} = \frac{u}{L}, \quad \tilde{v} = \frac{v}{L}, \quad \lambda = \frac{c_2}{c_1}, \quad \mu = \frac{c_1}{\alpha L} \quad \text{and} \quad \tilde{G} = \frac{GL^2}{c_1^2}. \tag{2.5}$$

where $c_2 = \sqrt{E_2/\rho}$.

The governing equations then become

$$\left.\begin{aligned}\frac{\partial^2\tilde{u}}{\partial\tilde{t}^2}-\frac{\partial^2\tilde{u}}{\partial\tilde{x}^2}-\frac{1}{\mu}\frac{\partial\tilde{v}}{\partial\tilde{t}}+\tilde{G}\tilde{u}=0,\\ \text{and}\qquad \frac{\partial^2\tilde{v}}{\partial\tilde{t}^2}-\lambda^2\frac{\partial^2\tilde{v}}{\partial\tilde{x}^2}+\frac{1}{\mu}\frac{\partial\tilde{u}}{\partial\tilde{t}}+\tilde{G}\tilde{v}=0,\end{aligned}\right\} \tag{2.6}$$

with initial conditions

$$\tilde{u}(\tilde{x},0)=f_1(\tilde{x}),\quad \tilde{v}(\tilde{x},0)=f_2(\tilde{x}),\quad \frac{\partial\tilde{u}}{\partial\tilde{t}}(\tilde{x},0)=g_1(\tilde{x})\quad\text{and}\quad \frac{\partial\tilde{v}}{\partial\tilde{t}}(\tilde{x},0)=g_2(\tilde{x}). \tag{2.7}$$

It may be noted that other scalings of the time variable are possible and an alternative will be considered in §3 in the regime of high gyricity and for small times. With the scaling above, μ is the parameter determined by the chirality and not gravity nor pre-stress, $\tilde{G}$ is the 'gravity' parameter, not affected by the chirality and pre-stress and λ is purely the pre-stress parameter. The other physical parameters may be regarded as fixed and having secondary importance for our purposes.

(c) The transient solution for finite chirality

For the case when the chiral rod is pre-stressed and experiences the effects of both gravity and a finite degree of chirality, the governing equations (2.6) with initial conditions (2.7) describe fully coupled chiral elastic waves moving under the force of gravity. The equations need to be solved numerically.

An illustration of this is shown in figure 1, where standard MATLAB software was used. The chirality and stiffness parameters are set to $\mu=1$ and $\lambda=0.5$, respectively, with the gravity parameter set as $\tilde{G}=10$. The rod is released from rest but with a non-zero initial longitudinal displacement and no transverse displacement. The initial conditions are:

$$\tilde{u}(\tilde{x},0)=\mathrm{e}^{-\tilde{x}^2},\quad \tilde{v}(\tilde{x},0)=0,\quad \frac{\partial\tilde{u}}{\partial\tilde{t}}(\tilde{x},0)=0\quad\text{and}\quad \frac{\partial\tilde{v}}{\partial\tilde{t}}(\tilde{x},0)=0. \tag{2.8}$$

A dimensionless time frame up to $\tilde{t}=12$ is chosen and an x domain is chosen sufficiently large such that the waves do not hit the boundary in this time frame. The longitudinal and transverse displacements are shown in figure 1*a*,*b*, respectively, as functions of x and t. Some representative orbits of points along the rod are shown in figure 1*c* and the position of the rod itself is shown in figure 1*d* at some representative times.

The chiral rod was released from rest with simply a displacement in the $\tilde{x}$-direction. Chirality has caused displacement at subsequent times in the direction perpendicular to the rod. From figure 1*d*, it is apparent that the initial wave profile is no longer preserved in time and there is evidence of dispersion.

For the remainder of this paper, the '~' will be omitted for convenience.

(d) Time harmonic solutions

Here, the special case of time harmonic solutions to the governing equations (2.6) will be considered. The governing equations simplify significantly, and the problem can be solved in a closed analytical form.

In the special case of time harmonic solutions of equation (2.6), we look for solutions of the form $u(x,t)=\mathcal{R}\rceil[A\exp(i(kx-\omega t))]$ and $v(x,t)=\mathcal{R}\rceil[B\exp(\mathrm{i}(kx-\omega t))]$, where A and B are, in

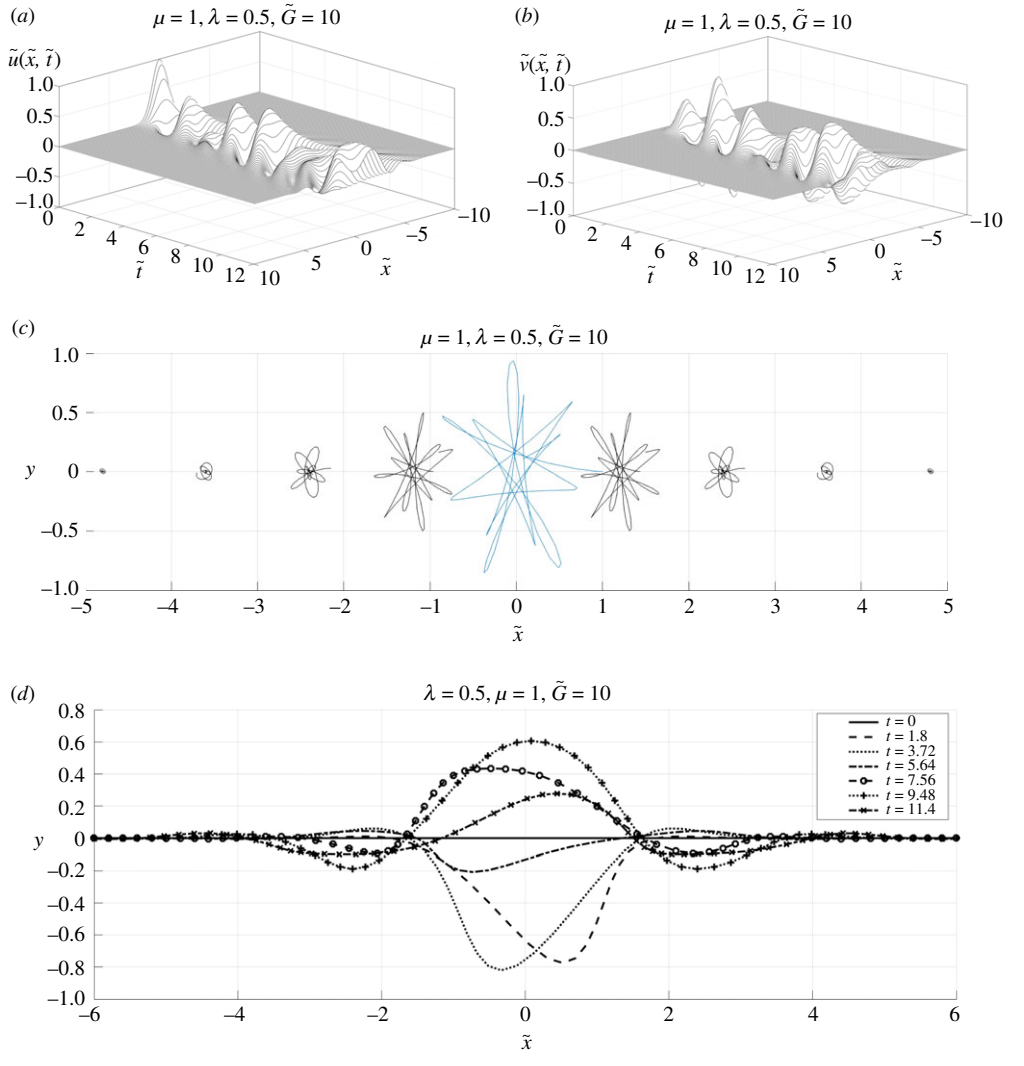

Figure 1. Transient motion of the chiral rod between $\tilde{t} = 0$ and $\tilde{t} = 12$. The pre-stress parameter $\lambda = 0.5$, the chirality parameter $\mu = 1$ and the gravity parameter $\tilde{G} = 10$, with the initial conditions (equation (2.8)). (*a*) The longitudinal displacement $\tilde{u}(\tilde{x}, \tilde{t})$. (*b*) The transverse displacement $\tilde{v}(\tilde{x}, \tilde{t})$. (*c*) The orbits of selected points of the chiral rod. (*d*) The chiral rod position at selected times.

general, complex phase-dependent constants, k is a wavenumber and ω an angular frequency (in dimensionless variables). Substituting these into equation (2.6) leads to the dispersion equation

$$\mu^2\omega^4 - (\mu^2\lambda^2k^2 + \mu^2k^2 + 2\mu^2G + 1)\omega^2 + (k^2 + G)(\lambda^2k^2 + G)\mu^2 = 0. \tag{2.9}$$

The solutions are given by

$$\omega_\pm^2(k, \mu, \lambda, G) = \frac{1 + (k^2\lambda^2 + k^2 + 2G)\mu^2 \pm \sqrt{1 + k^4(1 - \lambda^2)^2\mu^4 + 2((\lambda^2 + 1)k^2 + 2G)\mu^2}}{2\mu^2}. \tag{2.10}$$

Thus, for fixed μ, λ and G, there are two dispersion curves, both symmetric about $k = 0$. Some typical dispersion curves are shown in figure 2 for varying values of the parameters G, μ and λ. At $k = 0$, $\omega_\pm$ is independent of λ. Decreasing μ for fixed λ and G, leads to increasing separation

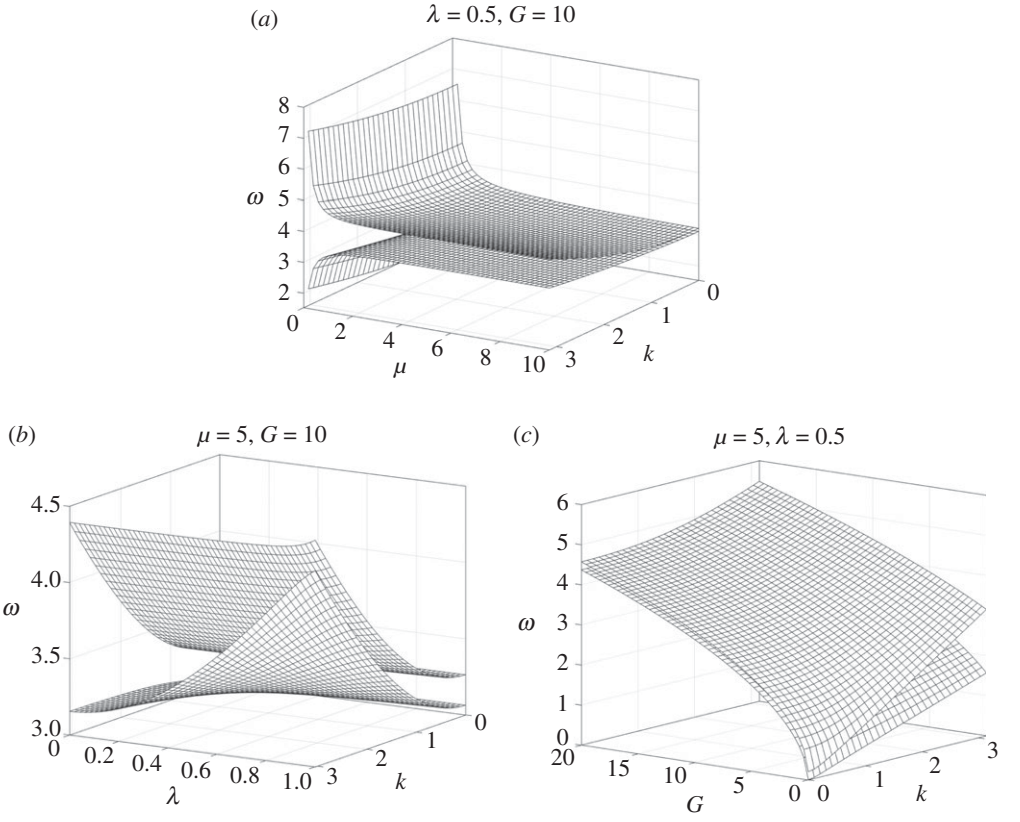

Figure 2. The effect of the varying values of the parameters μ, λ and G on the dispersion curves $\omega_{\pm}(k, \mu, \lambda, G)$. (*a*) The dispersion curves $\omega_{\pm}(k, \mu, 0.5, 10)$. (*b*) The dispersion curves $\omega_{\pm}(k, 5, \lambda, 10)$. (*c*) The dispersion curves $\omega_{\pm}(k, 5, 0.5, G)$.

of the modes with ω_+ increasing without limit ($\omega_+ \sim 1/\mu$) and ω_- decreasing to zero as $\mu \to 0$. Additionally, when G is non zero, there is a zero-level band gap which is not present in the absence of gravity. As $\mu \to \infty$ (corresponding to the case of zero gyricity), the dispersion curves coalesce to the single dispersion curve $\omega_{\pm} = \sqrt{1 + k^2}$ as expected. When both $G = 0$ and $\lambda = 0$, only one dispersion mode occurs.

The ratio of the amplitudes $\mathcal{R}_{\pm} = (B/A)_{\pm}$ corresponding to the modes with frequency $\omega_{\pm}$ are given by

$$\mathcal{R}_{\pm}(k, \mu, \lambda, G) = i\frac{\mu(k^2 - \omega_{\pm}(k, \mu, \lambda, G)^2 + G)}{\omega_{\pm}(k, \mu, \lambda, G)}. \tag{2.11}$$

Since the ratio of the amplitudes is purely imaginary, points along the chiral rod all move in standard elliptical orbits with their axes aligned with the rod and perpendicular to the rod. The equations of the orbits are given by

$$x'^2 + \left(\frac{y'}{\mathrm{Im}(\mathcal{R}_{\pm})}\right)^2 = 1, \tag{2.12}$$

where (x', y') are local displacement coordinates of a particle corresponding to the parallel and perpendicular directions to the rod, respectively, but with origin at the centre of the ellipses. The particles move in elliptical orbits in opposite directions for the two modes.

Thus, the eccentricity of the ellipses are determined by the behaviour of the functions $|\mathcal{R}_{\pm}(k, \mu, \lambda, G)|$. The variation of the functions $|\mathcal{R}_{\pm}(k, \mu, \lambda, G)|$ with μ, G and λ is shown in figure 3

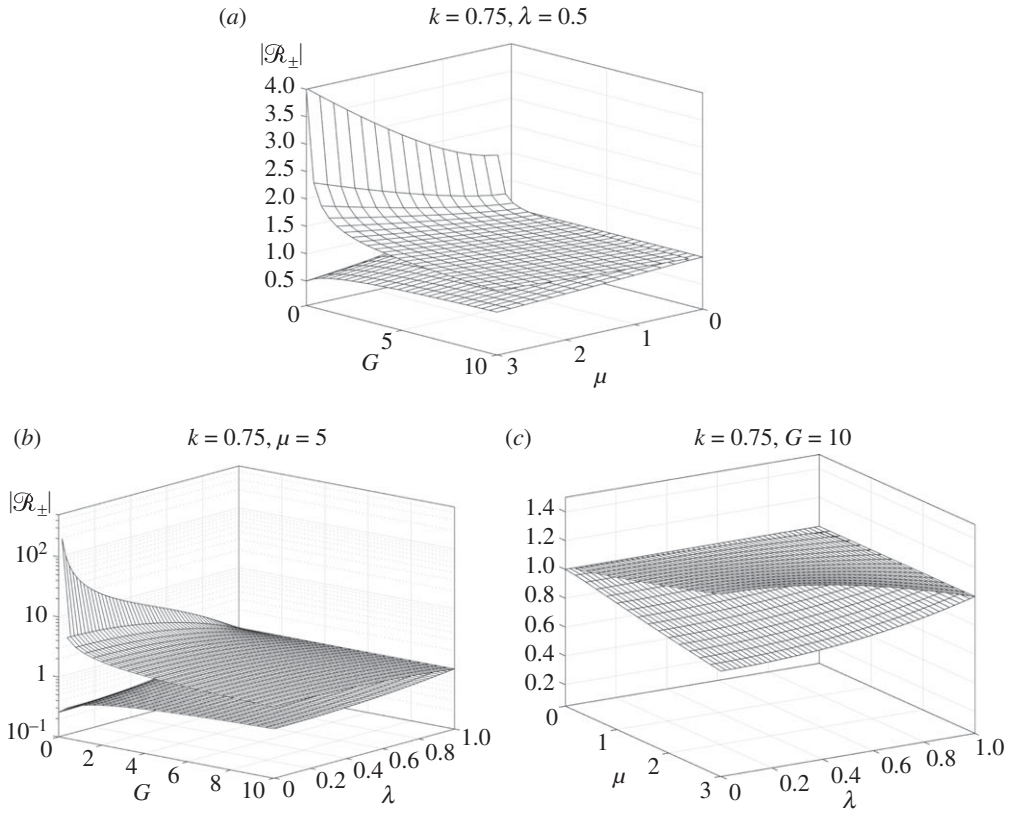

Figure 3. The variation in the eccentricity-related function $\mathcal{R}_{\pm}(k, \mu, \lambda, G)$ with each pair of the parameters μ, G and λ for a representative value of $k = 0.75$. In each case, the 'third' parameter has value $\lambda = 0.5$, $\mu = 5$, $G = 10$. (*a*) The function $\mathcal{R}_{\pm}(0.75, \mu, 0.5, G)$. (*b*) The function $\mathcal{R}_{\pm}(0.75, 5, \lambda, G)$. (*c*) The function $\mathcal{R}_{\pm}(0.75, \mu, \lambda, 10)$.

for a representative value of $k = 0.75$. In the figure, there is a boundary between the two modes represented by the plane

$$|\mathcal{R}_{\pm}(k, \mu, \lambda, G)| = 1. \tag{2.13}$$

This may be thought of as a 'purely chiral boundary' in that all modes with parameters, such that equation (2.13) holds, are degenerate with the orbits given as circles. As $\mu \to 0$, one circular mode only remains for all values of k, λ, μ and G. Circular orbits may be found in the limit $\lambda \to 1$, corresponding to very high pre-stress.

For the general situation when $\mu > 0$, $G > 0$ and $0 < \alpha < 1$, there are two elliptical orbits, with major axes aligned to the longitudinal and transverse axes of the chiral rod. This feature of ellipses being aligned only in the longitudinal or transverse directions was noted in the analysis of the chiral rod in the absence of gravity in [1] and in discrete chiral chains in [10].

For a particular choice of values for μ, G and λ then the two functions $\mathcal{R}_{\pm}(k, \mu, \lambda, G)$ will determine the shapes of the two standard ellipses. As in the calculations for figure 3, a representative value of $k = 0.75$ is considered. These two ellipses are shown as functions of each of three parameters μ, G and λ in figure 4. The ellipses are determined by equation (2.12). The ellipses are cut away for ease of viewing. It may be seen that there are single mode circular orbits in figure 4*a*,*c* in the limits $\mu \to 0$ and $\lambda \to 1$, respectively. It is not possible to design circular orbits through the control of the parameter G with μ and λ fixed.

An example of the chiral rod profiles for the 'plus' and 'minus' modes together with the orbits of three representative points on the rod are shown in figure 5. It should be noted that the eigenvectors determining the mode shapes are unique only up to the ratio of their amplitudes

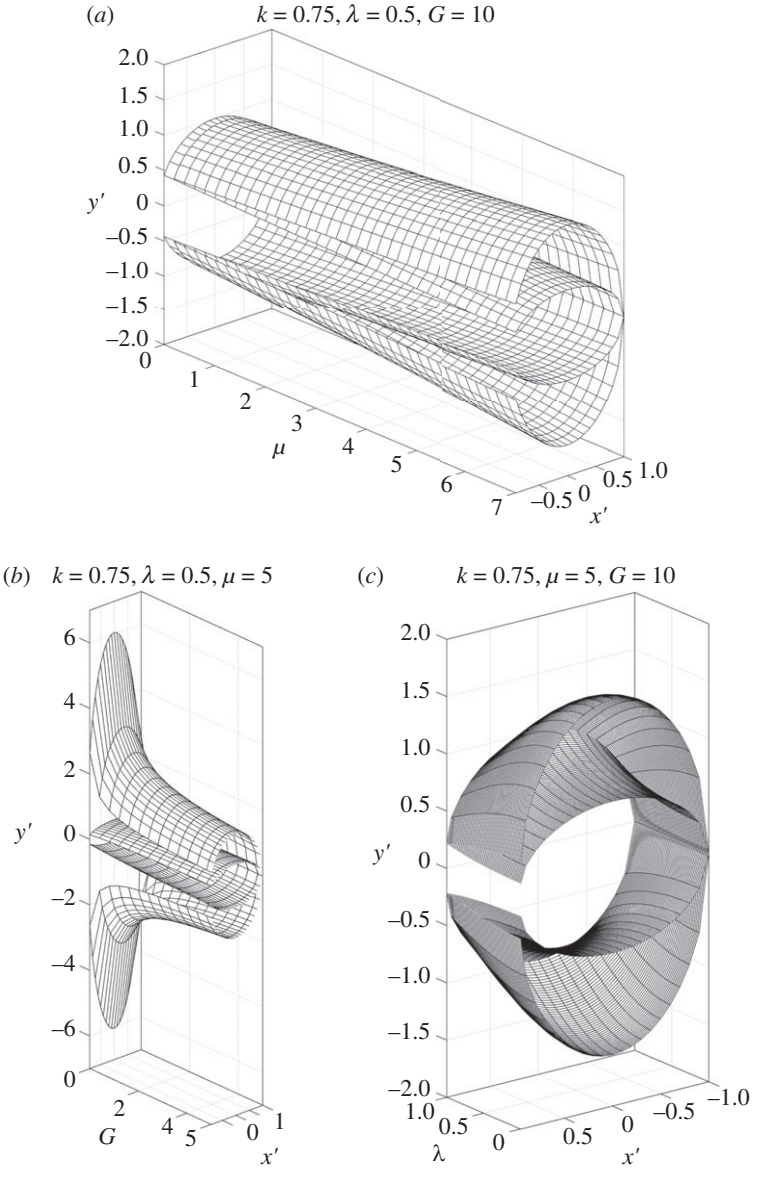

Figure 4. The two standard ellipses, referred to local coordinates x' and y', for the two modes shown as continuously changing with the parameters μ, G and λ. (*a*) The variation in the two standard ellipses with the gyricity parameter μ. (*b*) The variation in the two standard ellipses with the gravity parameter G. (*c*) The variation in the two standard ellipses with the pre-stress parameter λ.

given in equation (2.11). Initially, the representative points are at positions $x = -4, x = 1, x = 2$. The orbits are plotted as time increases until, after one-fifth of the period, the positions of every point on the rod are calculated and joined by a black line. The orbits are plotted as time continues until two-fifths of the period have passed and again the positions of every point on the rod are calculated and joined by a black line. This process is continued for one period. The five lines indicate the travelling wave. The orbits of the 'plus' mode rotate clockwise and the 'minus' mode anticlockwise. However, both waves move to the right as is expected from the dispersion relation at the chosen value of $k = 0.75$. The other parameters have values in both cases of $\lambda = 0.5$, $\mu = 5$, $G = 10$.

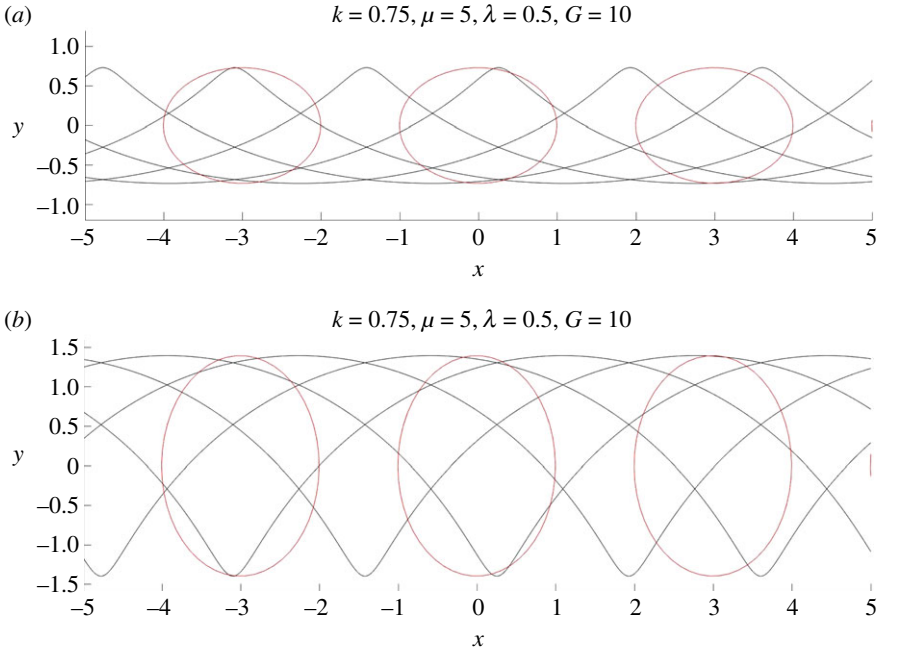

Figure 5. The chiral rod profiles for the 'plus' and 'minus' modes together with the orbits of three points on the rod, initially at positions $x = -4, x = 1, x = 2$. The 'plus' mode rotates clockwise and the 'minus' mode anticlockwise. The parameter values in both cases are $\lambda = 0.5, \mu = 5, G = 10$. (*a*) The 'plus' mode. (*b*) The 'minus' mode.

3. The case of high gyricity

When gyricity α increases, while c_1 and L in the normalization equation (2.5) remain fixed, the non-dimensional parameter μ becomes small.

In this case, we introduce the 'fast' time variable $T = t/\mu$ (t being the original dimensioned variable for time). Then equations (2.6) can be re-written in the form

$$\left.\begin{aligned} \frac{\partial^2 u}{\partial T^2} - \frac{\partial v}{\partial T} - \mu^2 \frac{\partial^2 u}{\partial x^2} + \mu^2 G u = 0 \\ \text{and} \quad \frac{\partial^2 v}{\partial T^2} + \frac{\partial u}{\partial T} - \mu^2 \lambda^2 \frac{\partial^2 v}{\partial x^2} + \mu^2 G v = 0, \end{aligned}\right\} \tag{3.1}$$

which suggests that on a finite interval of values of T, which is a small time interval if measured in terms of t, the spatial variation of u and v will be small, so that they can be approximated as functions of T only.

It is also noted that the gravity terms $\mu^2 G u, \mu^2 G v$ appear to be small when G is fixed, while $\mu \to 0$.

(a) The competition between the gravity and chirality

To observe a possible competition between the gravity and chirality, in the regime when $|\mu| \ll 1$, we introduce the quantity

$$\mathcal{G} = \mu^2 G.$$

The system (3.1) can be re-written in the form

$$\left.\begin{aligned}\frac{\partial^2 u}{\partial T^2}-\frac{\partial v}{\partial T}+\mathcal{G}u-\mu^2\frac{\partial^2 u}{\partial x^2}=0\\ \text{and}\qquad \frac{\partial^2 v}{\partial T^2}+\frac{\partial u}{\partial T}+\mathcal{G}v-\mu^2\lambda^2\frac{\partial^2 v}{\partial x^2}=0.\end{aligned}\right\} \tag{3.2}$$

It is also assumed that, while the initial displacements are finite, the initial velocities ($g_j,\ j=1,2$) may be large, i.e.

$$u(x,0)=f_1(x),\quad v(x,0)=f_2(x),\quad \frac{\partial u}{\partial T}(x,0)=\mathfrak{g}_1(x)\quad\text{and}\quad \frac{\partial v}{\partial T}(x,0)=\mathfrak{g}_2(x), \tag{3.3}$$

where $\mathfrak{g}_j(x)=\mu g_j,\ j=1,2$ are finite.

(b) The stationary wave limit

The case where chirality is very large, and $\mu\to 0$, has been considered in [1] where it is shown that the individual displacement fields maintain their original shape but these oscillate in time with a single characteristic frequency. Each point on the chiral rod oscillates in a circular trajectory. The gyricity now influences the parameter $\mathcal{G}$. For the present case with gravity, equations (3.2) with initial conditions (3.3) with $\mu=0$ have analytical solutions given by

$$\begin{aligned}u(x,T)=\frac{1}{2\Gamma}\Bigg[&A^+(x)\cos\left(\frac{\omega^- T}{2}\right)+A^-(x)\cos\left(\frac{\omega^+ T}{2}\right)\\&-\frac{4B^-(x)}{\omega^-}\sin\left(\frac{\omega^- T}{2}\right)+\frac{4B^+(x)}{\omega^+}\sin\left(\frac{\omega^+ T}{2}\right)\Bigg]\end{aligned} \tag{3.4}$$

and

$$\begin{aligned}v(x,T)=\frac{2}{\Gamma}\Bigg[&\frac{C^+(x)}{\omega^+}\sin\left(\frac{\omega^- T}{2}\right)+\frac{C^-(x)}{\omega^-}\sin\left(\frac{\omega^+ T}{2}\right)\\&+\frac{D^+(x)}{4}\cos\left(\frac{\omega^- T}{2}\right)+\frac{D^-(x)}{4}\cos\left(\frac{\omega^+ T}{2}\right)\Bigg],\end{aligned} \tag{3.5}$$

where $\Gamma=\sqrt{4\mathcal{G}+1}$ and $\omega^\pm=\Gamma\pm 1$ with

$$A^\pm(x)=\omega^\pm f_1(x)\pm 2\mathfrak{g}_2(x), \tag{3.6}$$

$$B^\pm(x)=\mathcal{G}f_2(x)\pm\frac{\omega^\pm\mathfrak{g}_1}{2}, \tag{3.7}$$

$$C^\pm(x)=\omega^\pm\left(\frac{f_1(x)+\mathfrak{g}_2(x)}{2}\right)\pm\mathcal{G}f_1(x) \tag{3.8}$$

and

$$D^\pm(x)=\omega^\pm f_2(x)\mp 2\mathfrak{g}_1(x). \tag{3.9}$$

From this solution, it may be seen that the presence of gravity has introduced an additional characteristic frequency, there being two frequencies $\omega^\pm$. Each point on the chiral rod moves in the same shape of orbit, which is non circular.

When the initial velocities are both zero and the initial displacement of either $u(x,T)$ or $v(x,T)$ is also zero, then the solution is separable in x and T indicating no dispersion.

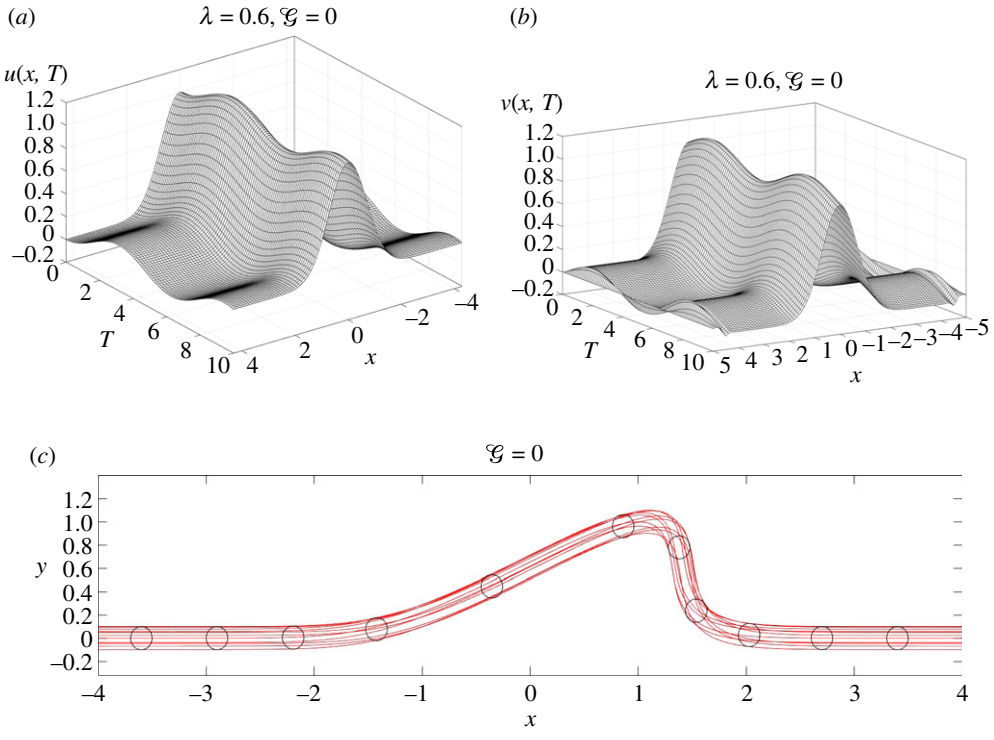

Figure 6. Motion of the chiral rod between $T = 0$ and $T = 10$ in the stationary wave limit. The pre-stress parameter $\lambda = 0.6$, and the gravity parameter $\mathcal{G} = 0$ (gravity neglected). (*a*) The longitudinal displacement $u(x, T)$. (*b*) The transverse displacement $v(x, T)$. (*c*) The displacement of the chiral rod at various times showing the orbits of a selection of points.

(c) Illustrative examples of the stationary wave solutions

An illustrative example of the stationary wave limit will now be given. The initial conditions for the calculations are

$$u(x,0) = v(x,0) = \mathrm{e}^{-x^2}, \quad \frac{\partial u}{\partial T}(x,0) = 0 \quad \text{and} \quad \frac{\partial v}{\partial T}(x,0) = 0.1. \tag{3.10}$$

With the pre-stress parameter $\lambda = 0.6$, the results for the case when $\mathcal{G} = 0$ are shown in figure 6 and may be compared with the corresponding results when the effect of gravity is included ($\mathcal{G} = 10$) in figure 7, both sets of results being taken over $0 \le T \le 10$.

As seen in figure 6*a*,*b*, the initial Gaussian profile is maintained throughout the subsequent motion but with amplitude varying with time. This is not the case when gravity is present as shown in figure 7*a*,*b*. The presence of the second non-zero frequency component, for the case when gravity is present, may also be seen in figure 7*a*,*b* with the increased number of 'ripples' in the direction of the T-axis. The orbits for each point along the chiral rod are circular when gravity is absent as may be seen in figure 6*c*. However, the presence of gravity changes the shape of the orbits considerably. In figure 7*c*, the orbits at selected points along the rod are plotted about a common centre for $0 \le T \le 10$. They are seen to be scaled versions of a common shape.

A few orbits for four representative points along the rod are plotted for $0 \le T \le 10$ in figure 7*d*. Initially, the representative points are at positions along the rod at $x = -3, x = -1, x = 1, x = 3$. The initial positions of *every* point on the rod are calculated and joined by a red line giving the initial displacement of the rod.

The orbits of the four representative points are plotted as time continues until $T = 1$. At this time, the positions of *every* point on the rod are calculated and joined by a red line giving the

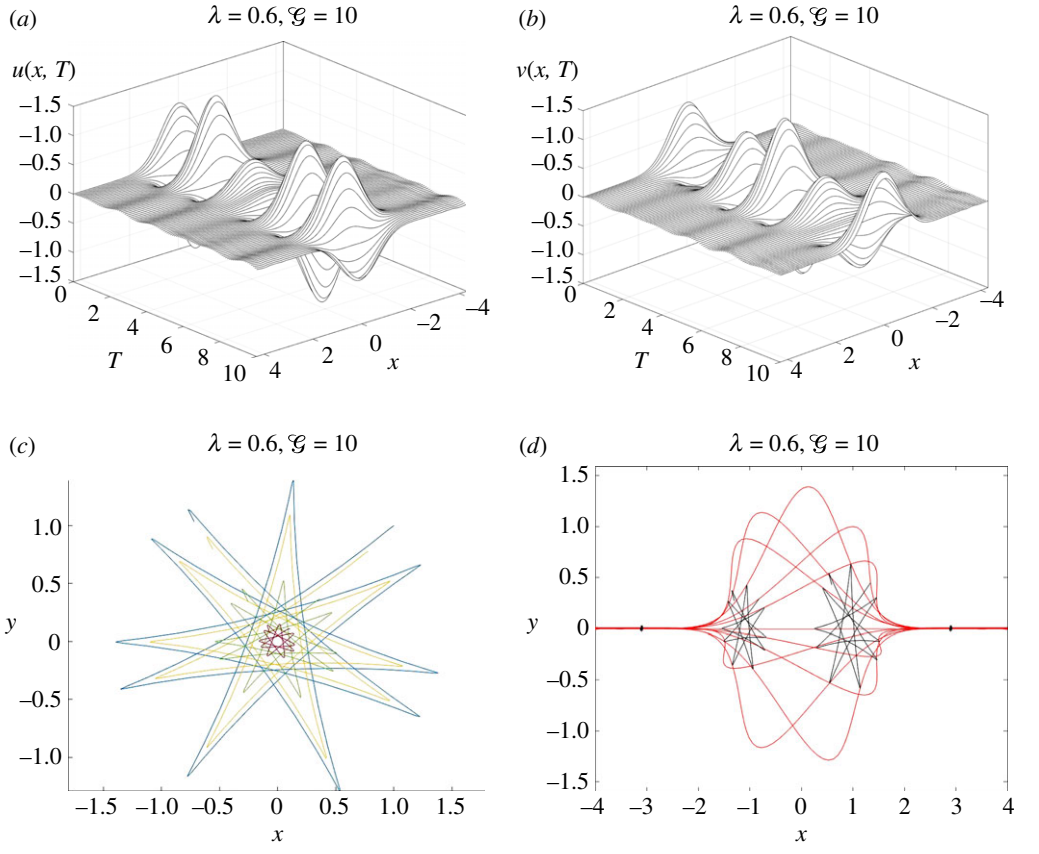

Figure 7. Motion of the chiral rod between $T = 0$ and $T = 10$ in the stationary wave limit. The pre-stress parameter $\lambda = 0.6$, and the gravity parameter $\mathcal{G} = 10$. (*a*) The longitudinal displacement $u(x, T)$. (*b*) The transverse displacement $v(x, T)$. (*c*) The orbits of selected points of the chiral rod plotted relative to a common central point. (*d*) The orbits of selected points on the chiral rod.

position of the rod at this time. This process is continued at every integer value of T up to $T = 10$. Note that the motion is not periodic in time (unless the ratio of the two frequencies is a rational number).

4. Transition regime for the case of a large gyricity

Here, we consider the transient case, when the dimensioned time interval is small ($0 \leq t \ll 1$ with t being the original dimensioned time), and when the displacements u and v are considered as functions of x, t and $T = t/\mu$, while μ is considered to be a small non-dimensional parameter:

$$|\mu| \ll 1.$$

In this section, the symbol 't' is used throughout for the original dimensioned time.

In the vector form, the system (2.6) is written as

$$\ddot{\mathbf{U}} - \mathbf{C}\frac{\partial^2}{\partial x^2}\mathbf{U} - \frac{1}{\mu}\mathbf{R}\dot{\mathbf{U}} + G\mathbf{U} = \mathbf{0}, \tag{4.1}$$

where

$$\mathbf{C} = \begin{pmatrix} 1 & 0 \\ 0 & \lambda^2 \end{pmatrix}, \quad \mathbf{R} = \begin{pmatrix} 0 & 1 \\ -1 & 0 \end{pmatrix} \quad \text{and} \quad \mathbf{U} = \begin{pmatrix} u \\ v \end{pmatrix}.$$

The initial conditions (equation (2.7)) are re-written as

$$\mathbf{U}(x,0)=\mathbf{f}=\begin{pmatrix} f_1(x)\\ f_2(x)\end{pmatrix} \quad \text{and} \quad \dot{\mathbf{U}}(x,0)=\mathbf{g}=\begin{pmatrix} g_1(x)\\ g_2(x)\end{pmatrix}. \tag{4.2}$$

In the transition regime, the vector function $\mathbf{U}$ characterizing the normalized vector of displacements, is assumed to depend on x, t and T:

$$\mathbf{U}=\mathbf{U}(x,t,T),$$

which yields

$$\dot{\mathbf{U}}=\frac{\partial}{\partial t}\mathbf{U}+\frac{1}{\mu}\frac{\partial}{\partial T}\mathbf{U},$$

and

$$\ddot{\mathbf{U}}=\frac{\partial^2}{\partial t^2}\mathbf{U}+\frac{2}{\mu}\frac{\partial^2}{\partial t\partial T}\mathbf{U}+\frac{1}{\mu^2}\frac{\partial^2}{\partial T^2}\mathbf{U}.$$

In this case, the vector equation (4.1) takes the form

$$\frac{\partial^2}{\partial T^2}\mathbf{U}-\mathbf{R}\frac{\partial}{\partial T}\mathbf{U}+\mu\left(2\frac{\partial^2}{\partial t\partial T}\mathbf{U}-\mathbf{R}\frac{\partial}{\partial t}\mathbf{U}\right)+\mu^2\left(\frac{\partial^2}{\partial t^2}\mathbf{U}-\mathbf{C}\frac{\partial^2}{\partial x^2}\mathbf{U}+G\mathbf{U}\right)=\mathbf{0}. \tag{4.3}$$

In addition, if the gravity parameter is large, i.e. $G=\mu^{-2}\mathcal{G}$, then the above equation becomes

$$\frac{\partial^2}{\partial T^2}\mathbf{U}-\mathbf{R}\frac{\partial}{\partial T}\mathbf{U}+\mathcal{G}\mathbf{U}+\mu\left(2\frac{\partial^2}{\partial t\partial T}\mathbf{U}-\mathbf{R}\frac{\partial}{\partial t}\mathbf{U}\right)+\mu^2\left(\frac{\partial^2}{\partial t^2}\mathbf{U}-\mathbf{C}\frac{\partial^2}{\partial x^2}\mathbf{U}\right)=\mathbf{0}. \tag{4.4}$$

(a) Asymptotic approximation. Boundary layer

When $0<t<\text{Const}\ \mu$, and $|\mu|\ll 1$ we show that the solution of the initial value problem, equations (4.1) and (4.2) may exhibit rapid temporal variation. Moreover, we distinguish between the case of finite gravity (see equation (4.3)), and the case when the gravity parameter G is large (see equation (4.4)). The term 'boundary layer' will be used here in connection to the terms, which depend on the fast-time variable $T=\mu^{-1}t$.

(i) The case of finite gravity

When the vector equation (4.3) holds, supplemented with the initial conditions (equation (4.2)), for the vector field $\mathbf{U}$, we consider the following asymptotic approximation:

$$\mathbf{U}\sim\mathbf{U}^{(0)}(x,t)+\mu\mathbf{U}^{(1)}(x,T), \tag{4.5}$$

where μ is the small non-dimensional parameter, and the approximation is considered on a small time interval $0\le t\ll 1$. To be more specific, we assume that $t=O(\mu)$.

Here, the first term $\mathbf{U}^{(0)}$ in equation (4.5) is a vector function of 'slow' variables (x,t), whereas the second term $\mathbf{U}^{(1)}$ is the boundary layer term, which represents a stationary wave limit field and depends on x and the 'fast' variable T.

The direct substitution of equation (4.5) into equation (4.3) gives

$$\mu\left(\frac{\partial^2}{\partial T^2}\mathbf{U}^{(1)}-\mathbf{R}\frac{\partial}{\partial T}\mathbf{U}^{(1)}-\mathbf{R}\frac{\partial}{\partial t}\mathbf{U}^{(0)}\right)+\mu^2\left(\frac{\partial^2}{\partial t^2}\mathbf{U}^{(0)}-\mathbf{C}\frac{\partial^2}{\partial x^2}\mathbf{U}^{(0)}+G\mathbf{U}^{(0)}\right)+O(\mu^3)=\mathbf{0}. \tag{4.6}$$

Also, the initial conditions (equation (4.2)) take the form

$$\left.\begin{aligned}&\mathbf{U}^{(0)}(x,0)+\mu\mathbf{U}^{(1)}+O(\mu^2)=\mathbf{f}\\ \text{and}\quad&\frac{\partial}{\partial t}\mathbf{U}^{(0)}(x,0)+\frac{\partial}{\partial T}\mathbf{U}^{(1)}(x,0)+O(\mu)=\mathbf{g},\end{aligned}\right\} \tag{4.7}$$

and, accordingly, we choose the functions $\mathbf{U}^{(0)}, \mathbf{U}^{(1)}$ to satisfy the initial conditions:

$$\mathbf{U}^{(0)}(x,0) = \mathbf{f}(x) \quad \text{and} \quad \frac{\partial \mathbf{U}^{(0)}}{\partial t}(x,0) = \mathbf{0} \tag{4.8}$$

and

$$\mathbf{U}^{(1)}(x,0) = \mathbf{0} \quad \text{and} \quad \frac{\partial \mathbf{U}^{(1)}}{\partial T}(x,0) = \mathbf{g}(x). \tag{4.9}$$

Furthermore, if on a small time-interval $0 < t < \text{Const}\,\mu$ the vector function $\mathbf{U}^{(0)}$ is approximated as

$$\mathbf{U}^{(0)}(x,t) = \mathbf{f}(x) + O(\mu^2),$$

then equation (4.6) can be re-written as follows:

$$\mu\left(\frac{\partial^2}{\partial T^2}\mathbf{U}^{(1)} - \mathbf{R}\frac{\partial}{\partial T}\mathbf{U}^{(1)}\right) + O(\mu^2) = \mathbf{0}. \tag{4.10}$$

Therefore, the boundary layer correction term corresponds to a stationary wave limit, already considered in the earlier §3b, and the vector function $\mathbf{U}^{(1)}(x,T)$ satisfies the equation

$$\frac{\partial^2}{\partial T^2}\mathbf{U}^{(1)} - \mathbf{R}\frac{\partial}{\partial T}\mathbf{U}^{(1)} = \mathbf{0}, \tag{4.11}$$

with the initial conditions (equation (4.9)). Using equations (3.4)–(3.9), with $\mathcal{G} = 0, \Gamma = 1$, $\omega^+ = 2, \omega^- = 0$, we deduce

$$\mathbf{U}^{(1)}(x,T) = 2\sin\left(\frac{T}{2}\right)\boldsymbol{\mathcal{M}}\left(-\frac{T}{2}\right)\mathbf{g}(x), \tag{4.12}$$

where the matrix function $\boldsymbol{\mathcal{M}}$ is defined by

$$\boldsymbol{\mathcal{M}}(T) = \begin{pmatrix} \cos(T) & -\sin(T) \\ \sin(T) & \cos(T) \end{pmatrix}, \tag{4.13}$$

and therefore

$$\mathbf{U}(x,t) \sim \mathbf{f}(x) + \mu\begin{pmatrix} g_1(x)\sin\left(\frac{t}{\mu}\right) + g_2(x)\left(1-\cos\left(\frac{t}{\mu}\right)\right) \\ g_2(x)\sin\left(\frac{t}{\mu}\right) - g_1(x)\left(1-\cos\left(\frac{t}{\mu}\right)\right) \end{pmatrix}. \tag{4.14}$$

We note that although the boundary layer correction term in equation (4.14) appears to be small, its time-derivative is of order $O(1)$.

A comparison between the numerical solution $u(0,t), v(0,t)$ of the governing equations (2.6), (2.7) and the asymptotic approximation equation (4.14), denoted by the suffix 'a' in the figure, is shown in figure 8*a* for small values of time. Here, we use the small parameter $\mu = 0.1$, finite value of the gravity parameter $G = 1$ and the parameter $\lambda = 0.5$ in the numerical solution. Good agreement is seen as $t = O(\mu)$, as predicted by the asymptotic model.

(ii) The case when the gravity is large

When $G = \mathcal{G}/\mu^2$, there are changes in the transition regime, when $0 < t < \text{Const}\,\mu$. In this case, the competition between the large parameter μ^{-1} (large gyricity) and large gravity parameter G is

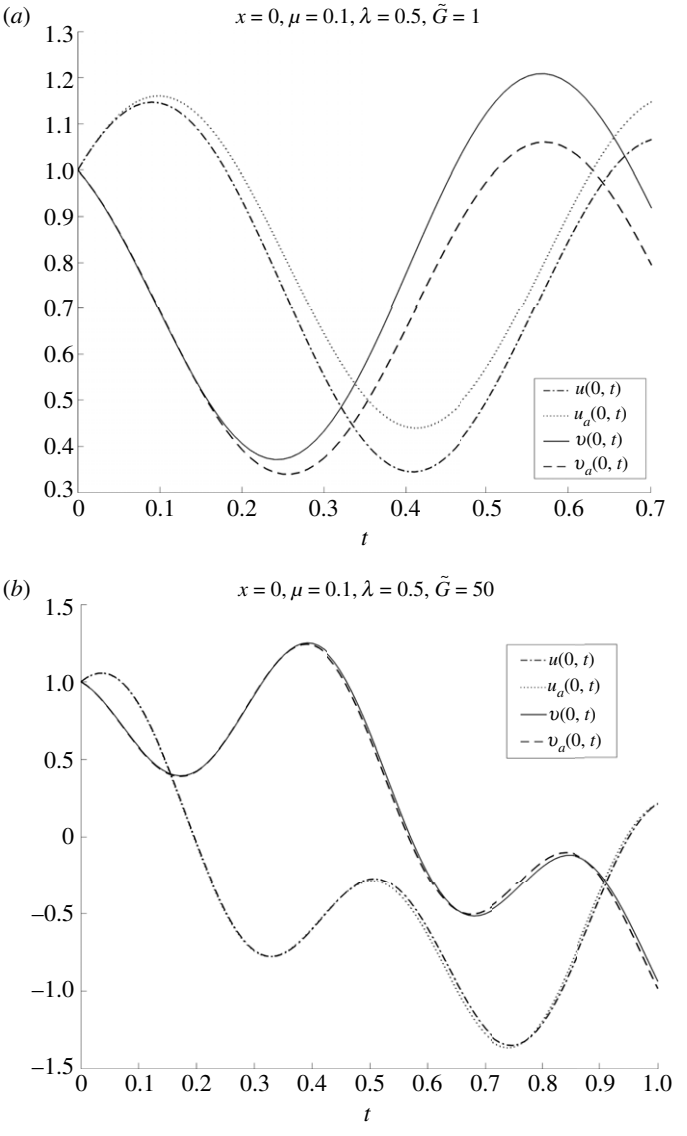

Figure 8. Comparison of the numerical solution $u(0,t)$, $v(0,t)$ of the governing equations (2.6), (2.7) and the asymptotic solutions for the cases of finite values (*a*) and large values (*b*) of the gravity parameter G. In both cases, the asymptotic values are denoted with a suffix '*a*' in the figure. The pre-stress parameter $\lambda = 0.5$ and the small chirality parameter $\mu = 0.1$ in both figures. (*a*) The numerical solutions for the longitudinal and transverse displacements versus the asymptotic approximations (equation (4.14)), for the case when $G = 1$. (*b*) The numerical solutions for the longitudinal and transverse displacements versus the asymptotic approximations (equation (4.29)), for the case of the large gravity parameter $G = 50$.

taken into account. The representation (equation (4.5)) will take the new form

$$\mathbf{U} \sim \mathbf{U}^{(0)}(x,T) + \mu \mathbf{U}^{(1)}(x,T), \tag{4.15}$$

where both vector functions $\mathbf{U}^{(0)}$ and $\mathbf{U}^{(1)}$ now depend on the fast variable $T = t/\mu$. By substituting equation (4.15) into equation (4.4) we deduce

$$\frac{\partial^2}{\partial T^2}\mathbf{U}^{(0)} - \mathbf{R}\frac{\partial}{\partial T}\mathbf{U}^{(0)} + \mathcal{G}\mathbf{U}^{(0)} + \mu\left(\frac{\partial^2}{\partial T^2}\mathbf{U}^{(1)} - \mathbf{R}\frac{\partial}{\partial T}\mathbf{U}^{(1)} + \mathcal{G}\mathbf{U}^{(1)}\right) + O(\mu^2) = \mathbf{0}, \tag{4.16}$$

with the initial conditions (equation (4.2)) taking the new form

$$\left.\begin{aligned}&\mathbf{U}^{(0)}(x,0)+\mu\mathbf{U}^{(1)}(x,0)+O(\mu^2)=\mathbf{f}\\ \text{and}\quad&\frac{1}{\mu}\frac{\partial}{\partial T}\mathbf{U}^{(0)}(x,0)+\frac{\partial}{\partial T}\mathbf{U}^{(1)}(x,0)+O(\mu)=\mathbf{g}.\end{aligned}\right\}\tag{4.17}$$

Accordingly, the initial conditions for the functions $\mathbf{U}^{(0)}(x,T)$ and $\mathbf{U}^{(1)}(x,T)$ are chosen as follows:

$$\mathbf{U}^{(0)}(x,0)=\mathbf{f}(x)\quad\text{and}\quad\frac{\partial\mathbf{U}^{(0)}}{\partial T}(x,0)=\mathbf{0},\tag{4.18}$$

and

$$\mathbf{U}^{(1)}(x,0)=\mathbf{0}\quad\text{and}\quad\frac{\partial\mathbf{U}^{(1)}}{\partial T}(x,0)=\mathbf{g}(x).\tag{4.19}$$

It follows from equation (4.16) that the leading-order term $\mathbf{U}^{(0)}$ satisfies the equation

$$\frac{\partial^2}{\partial T^2}\mathbf{U}^{(0)}-\mathbf{R}\frac{\partial}{\partial T}\mathbf{U}^{(0)}+\mathcal{G}\mathbf{U}^{(0)}=\mathbf{0},\tag{4.20}$$

together with the initial conditions (equation (4.18)). According to equations (3.4)–(3.9), the solution of this initial value problem is

$$\mathbf{U}^{(0)}(x,T)=\frac{1}{\Gamma}\mathbf{A}^{(0)}(T)\mathbf{f}(x),\tag{4.21}$$

where the matrix function $\mathbf{A}^{(0)}(T)$ is defined by

$$\mathbf{A}^{(0)}(T)=\frac{1}{2}\begin{pmatrix}\omega^+\cos\left(\frac{\omega^-T}{2}\right)+\omega^-\cos\left(\frac{\omega^+T}{2}\right) & \omega^-\sin\left(\frac{\omega^+T}{2}\right)-\omega^+\sin\left(\frac{\omega^-T}{2}\right)\\ \omega^+\sin\left(\frac{\omega^-T}{2}\right)-\omega^-\sin\left(\frac{\omega^+T}{2}\right) & \omega^+\cos\left(\frac{\omega^-T}{2}\right)+\omega^-\cos\left(\frac{\omega^+T}{2}\right)\end{pmatrix},\tag{4.22}$$

and

$$\omega^{\pm}=\Gamma\pm1\quad\text{and}\quad\Gamma=\sqrt{4\mathcal{G}+1}.\tag{4.23}$$

Therefore, the equivalent representation of $\mathbf{U}^{(0)}(x,T)$ is

$$\mathbf{U}^{(0)}=\left\{\cos\left(\frac{\Gamma T}{2}\right)\mathbf{I}-\frac{1}{\Gamma}\sin\left(\frac{\Gamma T}{2}\right)\mathbf{R}\right\}\boldsymbol{\mathcal{M}}\left(-\frac{T}{2}\right)\mathbf{f}(x),\tag{4.24}$$

where $\mathbf{I}$ is the identity matrix, and the rotation matrices $\mathbf{R}$ and $\boldsymbol{\mathcal{M}}$ are defined by equations (2.2) and (4.13), respectively.

Similarly, the vector function $\mathbf{U}^{(1)}(x,T)$ satisfies the equation

$$\frac{\partial^2}{\partial T^2}\mathbf{U}^{(1)}-\mathbf{R}\frac{\partial}{\partial T}\mathbf{U}^{(1)}+\mathcal{G}\mathbf{U}^{(1)}=\mathbf{0},\tag{4.25}$$

subject to the initial conditions (equation (4.19)). The solution of this initial value problem has the form (see equations (3.4)–(3.9))

$$\mathbf{U}^{(1)}(x,T)=\frac{1}{\Gamma}\mathbf{A}^{(1)}(T)\mathbf{g}(x),\tag{4.26}$$

where

$$\mathbf{A}^{(1)}(T)=\begin{pmatrix}\sin\left(\frac{\omega^-T}{2}\right)+\sin\left(\frac{\omega^+T}{2}\right) & \cos\left(\frac{\omega^-T}{2}\right)-\cos\left(\frac{\omega^+T}{2}\right)\\ \cos\left(\frac{\omega^+T}{2}\right)-\cos\left(\frac{\omega^-T}{2}\right) & \sin\left(\frac{\omega^-T}{2}\right)+\sin\left(\frac{\omega^+T}{2}\right)\end{pmatrix},\tag{4.27}$$

or equivalently

$$\mathbf{U}^{(1)}(x,T)=\frac{2}{\Gamma}\sin\left(\frac{\Gamma T}{2}\right)\boldsymbol{\mathcal{M}}\left(-\frac{T}{2}\right)\mathbf{g}(x),\tag{4.28}$$

where the rotation matrix function $\boldsymbol{\mathcal{M}}$ is defined in equation (4.13). We also note that equation (4.28) reduces to equation (4.12) when $\Gamma=1$.

Finally, we deduce that when the gravity is large, and μ is small, in the transition regime when $0\le t\ll1$, the displacement along the chiral waveguide corresponds to the stationary wave limit,

described by equations (3.4), (3.5), and the asymptotic approximation of $\mathbf{U}(x,t)$ can be re-written in the form

$$\mathbf{U}(x,t) \sim \frac{1}{\Gamma}\left(\mathbf{A}^{(0)}\left(\frac{t}{\mu}\right)\mathbf{f}(x) + \mu\mathbf{A}^{(1)}\left(\frac{t}{\mu}\right)\mathbf{g}(x)\right), \tag{4.29}$$

where the matrix functions $\mathbf{A}^{(0)}, \mathbf{A}^{(1)}$ are defined by equations (4.22) and (4.27), respectively.

We also note that, the formulae (4.24) and (4.28) show a certain structure, which incorporates the parameter Γ, depending on gravity, into a matrix factor in front of the rotation matrix function $\boldsymbol{\mathcal{M}}(-T/2)$.

A comparison between the numerical solution $u(0,t), v(0,t)$ of the governing equations (2.6), (2.7) and the asymptotic solution (equation (4.29)) (denoted by the suffix 'a' in the figure), is shown in figure 8*b* for the time interval corresponding to the transition regime. We use the small parameter $\mu = 0.1$, the large gravity parameter $G = 50$ and the parameter $\lambda = 0.5$ in the numerical solution. Excellent agreement is seen in figure 8*b* between the numerical solution and the asymptotic approximation (equation (4.29)).

(b) A temporal chiral interface of high gyricity

The problem of imperfect temporal chiral interface, without gravity, was analysed in [20].

In the presence of gravity, the vector equation of motion (equation (4.1)) takes the form

$$\frac{\partial}{\partial t}\left(\boldsymbol{\mathcal{M}}\left(\frac{t}{\mu}\right)\frac{\partial}{\partial t}\mathbf{U}(x,t)\right) - \boldsymbol{\mathcal{M}}\left(\frac{t}{\mu}\right)\mathbf{C}\frac{\partial^2}{\partial x^2}\mathbf{U}(x,t) + G\boldsymbol{\mathcal{M}}\left(\frac{t}{\mu}\right)\mathbf{U}(x,t) = \mathbf{0}, \tag{4.30}$$

where the rotation matrix function $\boldsymbol{\mathcal{M}}$ is defined by equation (4.13). Here, μ may change instantaneously across a temporal interface $t = T_*$, while the finite gravity parameter G is constant. It is also assumed that the displacement and the momentum remain continuous across the interface:

$$[\mathbf{U}]_{t=T_*-0}^{t=T_*+0} = \mathbf{0} \quad \text{and} \quad \left[\boldsymbol{\mathcal{M}}\left(\frac{t}{\mu}\right)\frac{\partial}{\partial t}\mathbf{U}\right]_{t=T_*-0}^{t=T_*+0} = \mathbf{0}. \tag{4.31}$$

We assume that at time $t = 0$, the gyricity switches from 0 to $\alpha \gg 1$, which corresponds to μ such that $|\mu| \ll 1$. At time $t = d > 0$, the gyricity switched back to zero. In this case, we consider the temporal interface $0 < t < d$. In particular, we are interested in the values of μ and d such that $|\mu| \ll 1$, while d/μ remains finite.

While outside the chiral interface, the displacement $\mathbf{U}$ satisfies the linear Klein–Gordon equation:

$$\ddot{\mathbf{U}} - \mathbf{C}\frac{\partial^2}{\partial x^2}\mathbf{U} + G\mathbf{U} = \mathbf{0}, \tag{4.32}$$

there are jump conditions across the chiral interface.

If we use the asymptotic approximation (equation (4.14)), across such a temporal interface, then we obtain the approximations for the jumps of the displacements and their derivatives:

$$[\mathbf{U}(x,t)]_{t=0-}^{t=d+0} \simeq \mu\begin{pmatrix} g_1(x)\sin\left(\frac{d}{\mu}\right) + g_2(x)\left(1-\cos\left(\frac{d}{\mu}\right)\right) \\ g_2(x)\sin\left(\frac{d}{\mu}\right) - g_1(x)\left(1-\cos\left(\frac{d}{\mu}\right)\right)\end{pmatrix}. \tag{4.33}$$

and

$$\left[\frac{\partial}{\partial t}\mathbf{U}(x,t)\right]_{t=0-}^{t=d+0} \simeq \left(\boldsymbol{\mathcal{M}}\left(\frac{d}{\mu}\right)\boldsymbol{\mathcal{M}}\left(-\frac{d}{\mu}\right) - \mathbf{I}\right)\begin{pmatrix} g_1(x) \\ g_2(x)\end{pmatrix} = \mathbf{0}. \tag{4.34}$$

The results demonstrate that for the temporal chiral interface, there is a small displacement jump. This jump is governed by the velocity $\mathbf{g}$ at time $t = 0-$. It is also observed that, when the gravity is finite, the jump conditions across the temporal chiral interface are not affected by gravity, and are similar to those studied in [20].

The applications of *the dynamic materials* with temporal interfaces are discussed in [15,19], and the wave patterns in such materials are also analysed in [16–18,20].

5. Concluding remarks

In the present paper, we have focused on the problem of wave propagation in a chiral meta-waveguide, subjected to gravity in addition to gyroscopic forces. We observe a gyroscopic coupling between the components of the displacement vector and gravity, in the context of the wave dispersion and wave localization.

An important part of the work is the analysis of the normalized governing equations, which incorporate non-dimensional displacements as well as the gyricity parameter and gravity, which emphasizes on the 'competition' between the gyroscopic chirality and gravity.

In particular, for the case when the gyroscopic gyricity is large, closed form analytical approximations of solutions have been derived in a given small time interval. It has also been demonstrated that when the normalized gravity parameter increases, the presence of gravity introduces an additional characteristic frequency in the wave pattern.

When the gyricity of the chiral system increases, we observe 'gyroscopic rigidity' in the transient context, i.e. the spatial advance of the elastic wave becomes negligibly small. In this case, the fast time-variable is used to describe the rapid oscillation of the mechanical system in some transitional regimes. Two classes of formulations have been analysed in the presence of gravity: the case of finite gravity and large gyroscopic chirality, and the case when gravity is finite and the gyroscopic chirality is large. The first case shows the 'frequency split' in the representation of the temporal boundary layer, compared to the second case. Finally, these results were used to derive the jump conditions across temporal chiral interfaces in an elastic wave guide, subjected to gravity.

Data accessibility. This article has no additional data.

Declaration of AI use. We have not used AI-assisted technologies in creating this article.

Authors' contributions. I.S.J.: conceptualization, data curation, formal analysis, investigation, writing—original draft, writing—review and editing; N.V.M.: conceptualization, data curation, formal analysis, investigation, writing—original draft, writing—review and editing; A.B.M.: conceptualization, data curation, formal analysis, investigation, writing—original draft, writing—review and editing.

All authors gave final approval for publication and agreed to be held accountable for the work performed therein.

Conflict of interest declaration. We declare we have no competing interests.

Funding. The paper was written when N.V.M. and A.B.M. visited the Isaac Newton Institute for Mathematical Sciences, Cambridge, attending the Multiple Wave Scattering programme, supported by EPSRC (grant no. EP/R014604/1).

Acknowledgements. I.S.J. is grateful to the Department of Mathematical Sciences,University of Liverpool and the Liverpool Research Centre for Mathematics and Modelling for the provision of the research infrastructure and computational facilities. N.V.M. and A.B.M. would like to thank the Isaac Newton Institute for Mathematical Sciences, Cambridge, for support and hospitality during the *Multiple Wave Scattering* programme where a part of the work on this paper was undertaken.

References

1. Jones IS, Movchan NV, Movchan AB. 2022 Chiral waves in structured elastic systems: dynamics of a meta-waveguide. *Q. J. Mech. Appl. Math.* **75**, 63–89. (doi:10.1093/qjmam/hbab015)
2. Carta G, Jones IS, Movchan NV, Movchan AB. 2019 Wave polarization and dynamic degeneracy in a chiral elastic lattice. *Proc. R. Soc. A* **475**, 20190313. (doi:10.1098/rspa.2019.0313)
3. Carta G, Jones IS, Movchan NV, Movchan AB. 2019 Wave characterisation in a dynamic elastic lattice: lattice flux and circulation. *Phys. Mesomech.* **22**, 152–163. (doi:10.1134/S102995991902005X)
4. Gray A. 1918 *A treatise on gyrostatics and rotational motion*. London, UK: McMillan and Co, Ltd.
5. Lorentz HA. 1895 *Versuch einer theorie der electrischen und optischen erscheinungen in bewegten Körpern*. Leiden, Germany: Leiden - E J Brill.
6. Landau LD, Lifshitz EM, Pitaevskii LP. 1984 *Electrodynamics of continuous media*. vol. 8, 2nd edn. *Course of theoretical physics*. Oxford, UK: Butterworth-Heinemann.

7. Brun M, Jones IS, Movchan AB. 2012 Vortex-type elastic structured media and dynamic shielding. *Proc. R. Soc. A* **468**, 3027–3046. (doi:10.1098/rspa.2012.0165)
8. Wang P, Lu L, Bertoldi K. 2015 Topological phononic crystals with one-way elastic edge waves. *Phys. Rev. Lett.* **115**, 104302. (doi:10.1103/PhysRevLett.115.104302)
9. Huber SD. 2016 Topological mechanics. *Nat. Phys.* **12**, 621–623. (doi:10.1038/nphys3801)
10. Jones IS, Movchan NV, Movchan AB. 2020 Two-dimensional waves in a chiral elastic chain: dynamic Green's matrices and localised defect modes. *Q. J. Mech. Appl. Math.* **73**, 305–328. (doi:10.1093/qjmam/hbaa014)
11. Kandiah A, Jones IS, Movchan NV, Movchan AB. 2023 Effect of gravity on the dispersion and wave localisation in gyroscopic elastic systems. In *Mechanics of heterogeneousmaterials. Advanced structured materials*, vol. 8611H (eds H Altenbach, G Bruno, VA Eremeyev, M Yu Gutkin, WH Mŭller), pp. 219–274. Berlin, Germany: Springer.
12. Carta G, Nieves MJ, Jones IS, Movchan NV, Movchan AB. 2018 Elastic chiral waveguides with gyro-hinges. *Q. J. Mech. Appl. Math.* **71**, 157–185. (doi:10.1093/qjmam/hby001)
13. Nieves MJ, Carta G, Jones IS, Movchan AB, Movchan NV. 2018 Vibrations and elastic waves in chiral multi-structures. *J. Mech. Phys. Solids* **121**, 387–408. (doi:10.1016/j.jmps.2018.07.020)
14. Carta G, Nieves MJ, Jones IS, Movchan NV, Movchan AB. 2019 Flexural vibration systems with gyroscopic spinners. *Phil. Trans. R. Soc. A* **377**, 20190154. (doi:10.1098/rsta.2019.0154)
15. Lurie KA. 2017 *An introduction to mathematical theory of dynamic materials*. Berlin, Germany: Springer.
16. Milton GW, Mattei O. 2017 Field patterns: a new mathematical object. *Proc. R. Soc. A* **473**, 20160819. (doi:10.1098/rspa.2016.0819)
17. Mattei O, Milton GW. 2017 Field patterns without blow up. *New J. Phys.* **19**, 093022. (doi:10.1088/1367-2630/aa847d)
18. Mattei O, Milton GW. 2017 Field patterns: a new type of wave with infinitely degenerate band structure. *Europhys. Lett.* **120**, 54003. (doi:10.1209/0295-5075/120/54003)
19. Lurie KA, Weekes SL. 2006 Wave propagation and energy exchange in a spatio-temporal material composite with rectangular microstructure. *J. Math. Anal. Appl.* **314**, 286–310. (doi:10.1016/j.jmaa.2005.03.093)
20. Movchan AB, Movchan NV, Jones IS, Milton GW, Nguyen H-M. 2022 Frontal waves and transmissions for temporal laminates and imperfect chiral interfaces. *Phil. Trans. R. Soc. A* **380**, 20210385. (doi:10.1098/rsta.2021.0385)